Contract No:

This document was prepared in conjunction with work accomplished under Contract No. DE-AC09-08SR22470 with the U.S. Department of Energy (DOE) Office of Environmental Management (EM).

Disclaimer:

Hybrid Fe_2O_3-Au Nanoparticles: Synthesis and Photothermal Properties

George K. Larsen[1] and Simona E. Hunyadi Murph[1, 2*]

[1]Savannah River National Laboratory, Aiken SC 29808, U.S.A., George.Larsen@srnl.doe.gov,
[2]Georgia Regents University, Augusta GA 30912, U.S.A., *Simona.Murph@srnl.doe.gov

ABSTRACT

We describe the synthesis and properites of hybrid Fe_2O_3-Au nanoparticles synthesized using a wet chemical approach. These nanoparticles are compared with Fe_2O_3 and Au nanoparticles prepared in corresponding manners. We investigate the visible light photothermal properties of these different nanoparticles. It is found that the hybrid Fe_2O_3-Au nanoparticles are able to photothermally heat aqueous solutions as efficiently as pure Au nanoparticles, even with a significantly smaller concentration of Au. Importantly, the hybrid structures retain the properties of both materials, creating a multifunctional structure with excellent magnetic and plasmonic properties.

Keywords: gold, iron oxide, multifunctional, plasmonics, hyperthermia

1 INTRODUCTION

A considerable amount of research has been devoted to studying the unique and tunable behavior of nanoparticles and to identifying novel applications for these properties [1]. Noble metal nanoparticles, especially gold nanoparticles, have received much of this attention due to the exhibition of localized surface plasmon resonances (LSPRs) [2]. LSPR is an intriguing phenomenon where free electrons in highly conductive noble metal nanoparticles collectively oscillate when resonantly driven by electromagnetic radiation. This process results in strong absorbance and scattering and can generate intense, highly confined electromagnetic fields. Such effects have enabled a wide variety of applications including chemical and biological sensing [3-5], plasmonic circuits [2], enhanced photocatalysts [6, 7], medical diagnostics [8, 9], and cancer therapy [10]. While these diverse applications are certainly remarkable, the functionality of nanoscale gold can be further enhanced through combination with other materials to create multicomponent or hybrid nanoparticles [11]. Hybrid nanoparticles take advantage of the physicochemical properties of two or more materials to create a new multifunctional composite nanostructure. For example, Au can be combined with a magnetic material to form nanoparticles that retain the interesting chemistry and plasmonic properties of Au, but can also interact with external magnetic fields, such as those used for magnetic resonance imaging (MRI) or for external manipulation [12].

Iron(III) oxide, Fe_2O_3, also makes an interesting component of multifunctional nanoparticles. Fe_2O_3 is an abundant, non-toxic semiconductor with a band gap in the visible region. As a single material, Fe_2O_3 nanomaterials have been used for photocatalysis [13], chemical sensors [14], MRI contrast agents [15], drug delivery [16], and magnetic hyperthermia [17]. Because of the latter three applications, the combination of Fe_2O_3 with Au is particularly attractive for biomedical applications. In fact, Au-Fe_2O_3 nanoparticles have demonstrated the ability to penetrate the plasma membrane of cells in an applied magnetic field and facilitate gene transfer through adenovirus delivery [18]. Another important biomedical application of Fe_2O_3-Au nanoparticles is that of cancer diagnosis and treatment through MRI and photothermal therapy [8]. In this case, Fe_2O_3 functions as an MRI contrast agent, while the Au portion locally converts incident infrared light to heat through dissipation of electromagnetic energy excited during LSPR absorbance. Despite the promise of photothermal therapy using magnetic Fe_2O_3-Au nanoparticles, very few studies have considered the light-induced effects of such hybrid nanoparticles outside of the infrared region.

In this report, we describe the synthesis and morphology of hybrid Fe_2O_3-Au nanoparticles synthesized using a wet chemical method. These nanoparticles are compared with pure Fe_2O_3 and Au nanoparticles that are prepared in corresponding manners. We investigate the visible light photothermal properties of these different nanoparticles. It is found that the hybrid Fe_2O_3-Au nanoparticles retain their magnetic properties and are able to photothermally heat aqueous solutions as efficiently as pure Au nanoparticles, even with a significantly smaller concentration of plasmonic material.

2 EXPERIMENTAL SECTION

Nanoparticle synthesis: Chloroauric acid trihydrate ($HAuCl_4*3H_2O$), trisodium citrate, and iron oxide (Fe_2O_3) were purchased from Sigma Aldrich. All chemicals were used as received. All glassware was cleaned with aqua regia and thoroughly rinsed with deionized water prior use. Gold nanospheres were prepared by a citrate reduction approach described elsewhere [4, 19]. With this synthesis, an aqueous solution of 2.5×10^{-4} M $HAuCl_4$ was heated to boiling and one percent by weight sodium citrate solution was subsequently added. The boiling was continued until the solution turned ruby red, indicating the formation of gold nanoparticles. Fe_2O_3-Au hybrid nanoparticles were prepared by a similar procedure by reducing the same

amount of Au^{3+} ions in the presence of 2.2×10^{-4} M Fe_2O_3 nanoparticles. The solutions of Au nanospheres and hybrid

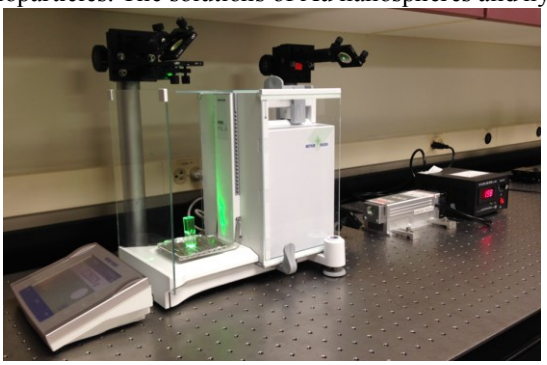

Figure 1: Photograph of photothermal heating system showing laser path, sample position, and microgram scale.

Fe_2O_3-Au were centrifuged twice at 7000 rpm for 5 minutes and redispersed in DI water to remove excess reactants.

Characterization: The morphology of the nanoparticles were observed by scanning electron microscopy (SEM, Hitachi S400). The nanoparticle size distribution and zeta potential were obtained using dynamic light scattering measurements (DLS, Brookhaven Instruments, NanoBrook Omni). The chemical compositions were analyzed using inductively coupled plasma mass spectrometry (ICP-MS, Agilent 7500s). The optical properties of the nanoparticle solutions were measured using UV-visible-near infrared spectroscopy (UV-Vis-NIR, Tec5 MultiSpec).

Photothermal experiment: The photothermal experimental setup (**Figure 1**) consists of a laser with wavelength λ = 532 nm (Del Mar Photonics, DMPV-532-1, beam diameter focused to ~20 μm at 1200 mW), where the beam path is directed onto the top surface of 3 mL nanoparticle solution contained in a methacrylate cuvette. The cuvette is resting on a microgram scale (Mettler Toledo XP205) that provides dynamic mass measurements. These data are synchronized with the bulk solution temperature data, which is obtained from an infrared thermocouple (Omega Engineering, OS801-HT). The data is logged using a custom LabVIEW program. A control experiment found no detectable temperature rise when pure deionized water is illuminated with the laser at test conditions. During the control experiment, the microgram scale only detected the ambient evaporation rate during, which is generally an order of magnitude smaller than the nanoparticle photothermal rate.

3 RESULTS AND DISCUSSION

The electron microscopy images of the Fe_2O_3 nanoparticles (**Figures 2a-b)** show rounded, irregular particles that tend to aggregate in clumps. Statistical analysis of the nanoparticles reveals that the average diameter of the Fe_2O_3 particles is d = 40 ± 10 nm. The SEM images of the hybrid Fe_2O_3-Au nanoparticles are shown in **Figures 2c-d**. Here, it can be observed that the original Fe_2O_3 nanoparticles remain mostly unchanged, except now they appear functionalized with smaller, bright, and rounded nanoparticles, which are identified as Au. In general, the Au nanoparticles are variously sized (d = 20 ± 20 nm) and are well dispersed.

The structural behavior of the nanoparticles in solution can be characterized by DLS measurements. The DLS results are summarized in **Table 1**, and it is found that the measured hydrodynamic radius is greater than that measured by SEM, as expected. The DLS measurements capture the aggregation behavior of the Fe_2O_3 particles, showing population bins with hydrodynamic radii of d_h = 95, 450, and 5500 nm. Interestingly, coupling Fe2O3 with Au reduces the aggregation behavior of the particles, as the hybrid Fe_2O_3-Au nanoparticles have population bins at d_h = 61 and 310 nm. In comparison, pure Au nanoparticles are well dispersed in solution, with a single population at d_h = 35 nm. The aggregation behavior of the different nanoparticles is consistent with the measured zeta potential. Fe_2O_3 nanoparticles have a zeta potential of ζ = -11 mV, while Fe_2O_3-Au particles have ζ = -16 mV, and Au particles have ζ = -30 mV. The original net negative charge is due to adsorbed citrate in the Au nanoparticles. The effective surface charge decrease of the Fe2O3-Au before and after

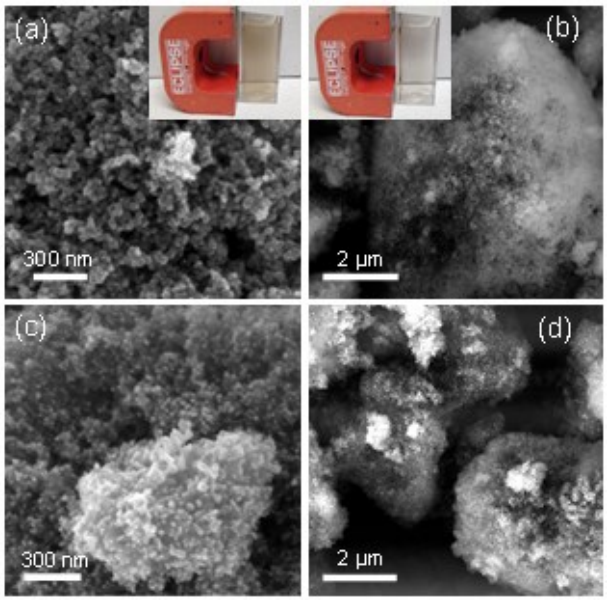

Figure 2: SEM images of (a)-(b) Fe_2O_3 nanoparticles and (c)-(d) hybrid Fe_eO_3-Au nanoparticles. Insets: Photographs of a hybrid Fe_2O_3-Au nanoparticle solution (a) before and (b) after magnetic separation.

	d_h, average (nm)	d_h, bin (nm)	Population (%)	zeta potential (mV)
Fe_2O_3	2265	95	8	-11
		450	39	
		5500	52	
Fe_2O_3-Au	243	61	13	-16
		310	87	
Au	35			-30

Table 1: Summary of the DLS experimental data

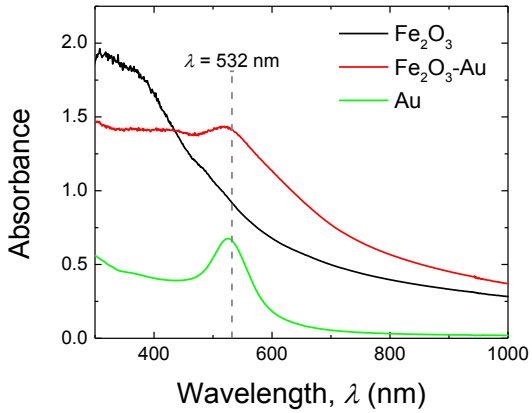

Figure 3: UV-vis absorbance spectra of the nanoparticles

coupling with Au is attributed to partial removal of citrate capping agent, in agreement with previous results [9].

ICP-MS data were obtained in order to quantitatively confirm the Au and Fe compositions of these nanoparticle solutions. The Fe_2O_3 nanoparticle solutions had a Fe concentration of ρ_{Fe} = 4400 ppb. The hybrid Fe_2O_3-Au nanoparticles had Fe and Au concentrations of ρ_{Fe} = 150 ppb and ρ_{Au} = 49 ppb, respectively. Finally, pure Au nanoparticles had concentrations of ρ_{Au} = 1100 ppb. The ICP-MS data confirms Au loading on the surface of the hybrid Fe_2O_3-Au nanoparticles at a value that is 20 times smaller than the control Au concentration. It is also worthwhile to note that the Au loading does not negatively affect the magnetic properties of the Fe_2O_3 nanoparticles. This can be observed in the insets in **Figure 2**. Initially, the Fe_2O_3-Au solution is brown but turns clear after a few minutes under magnetic manipulation since all of the nanoparticles are magnetic and are contained by the field.

In order to determine the optical properties of the different nanoparticle solutions, UV-vis-NIR absorbance spectra were acquired (**Figure 3**). The Fe_2O_3 nanoparticles absorb across much of the UV-visible-NIR region, with a distinct increase occurring for λ < 600 nm as the band gap is approached. For the hybrid Fe_2O_3-Au nanoparticles, a similar behavior is observed, except there is a noticeable peak centered around $\lambda \approx$ 520 nm, which is attributed to the LSPR of the Au nanoparticles. This attribution is substantiated by comparison with the measured absorbance spectrum of the Au nanoparticles. The Au nanoparticles have a distinct LSPR absorbance peak centered around $\lambda \approx$ 525 nm. Thus, the spectrum of the hybrid Fe_2O_3-Au nanoparticles includes contributions from the two individual materials, Fe_2O_3 and nanoscale Au, though the slight blue-shift in the LSPR indicates that the hybrid nanomaterials are not behaving as a simple mixture of the constituent materials.

The photothermal heating results are presented in **Figure 4a**. For all nanoparticle solutions, a significant temperature rise is observed after the laser is turned on at time, t = 120 s. In general, the bulk temperature increases exponentially and approaches an equilibrium value until the laser is turned off at t = 1120 s. These temperature profiles

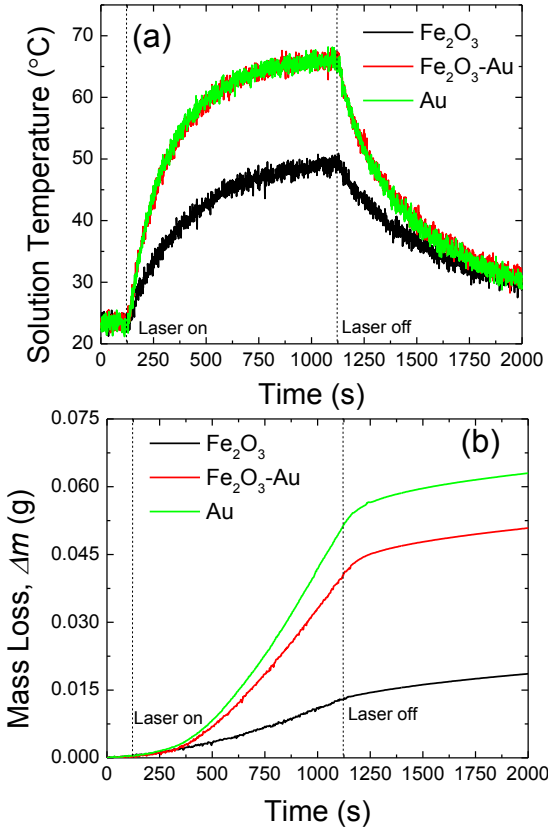

Figure 4: Photothermal experimental results: (a) solution temperature and (b) mass loss as a function of time.

are consistent with heat diffusion occurring in a dissipative medium [20]. For the Fe_2O_3 nanoparticles, the maximum bulk temperature achieved during the experiment is T_{max} = 50 ºC, which is the lowest of the three particle types tested. Interestingly, the hybrid Fe_2O_3-Au nanoparticles and Au nanoparticles have very similar temperature profiles, with both nanoparticle solutions achieving T_{max} = 68 ºC. It is important to note that magnitude of absorbance at the laser wavelength, $\lambda \approx$ 532 nm, does not directly relate to T_{max} in these cases. This is most likely due to plasmonic effects arising when Au is present. That is, well-separated, non-interacting nanoparticles, e.g., Fe_2O_3 nanoparticles, solely transduce heat from light via their absorption cross-section. However, closely spaced plasmonic nanoparticle aggregates can exhibit local hot spots where the electric field and corresponding heating intensity can be greatly enhanced [21]. It is expected that these plasmonic hot spots contribute to the larger T_{max} observed when Au is present. Furthermore, increased plasmonic interactions might contribute to the relatively efficient heating in the hybrid Fe_2O_3-Au nanoparticle solution, which has a smaller Au concentration but increased aggregation, as indicated by ICP-MS and DLS, respectively.

Finally, it is interesting to observe the change in the nanoparticle solutions' mass as a function of time under

laser illumination, as this is related to the steam generation rate. The results are given in **Figure 4b**, which plots the mass loss during the photothermal experiments. In general, all nanoparticle solutions exhibit obvious decreases in mass, which suggests that the temperature in the irradiated region is hot enough to generate steam. Similar to the temperature profiles (**Figure 4a**), the mass loss increases exponentially after the laser is turned on and approaches a steady state value until the laser is turned off. This steady state mass loss, Δm, is found by measuring the slope of the linear region of the curve. For Fe_2O_3 nanoparticles, $\Delta m = 1.656 \pm 0.005 \times 10^{-5}$ g/s, and for the hybrid Fe_2O_3-Au nanoparticles, $\Delta m = 5.72 \pm 0.01 \times 10^{-5}$ g/s. In spite of their identical temperature profiles, Au nanoparticles exhibit greater mass loss than hybrid Fe_2O_3-Au nanoparticles; $\Delta m = 7.44 \pm 0.02 \times 10^{-5}$ g/s for the Au nanoparticles. In other words, both nanoparticle solutions exhibit the same temperature as a function of time and reach the same maximum temperature, yet the Au nanoparticle solution loses mass slightly more rapidly than the hybrid Fe_2O_3-Au nanoparticles. This suggests that LSPRs might play additional roles (*i.e.*, hot electron injection [22]) beyond photothermal heating in the phase change related mass loss of the solutions, and these effects are less pronounced in the hybrid Fe_2O_3-Au nanoparticle solutions due to the smaller Au loading. This is an interesting result which needs further study. In general, though, the photothermal experiments show the benefits of creating multifunctional materials: even a significantly smaller Au loading on Fe_2O_3 leads to virtually the same heating effects as pure Au, and at the same time, the magnetic functionality of the Fe_2O_3 can be used for MRI imaging or magnetic manipulation, greatly expanding the material's utility.

4 CONCLUSION

We have synthesized hybrid Fe_2O_3-Au nanoparticle solutions and compared their properties with corresponding single material nanoparticle solutions of Fe_2O_3 and Au. The hybrid Fe_2O_3-Au nanoparticles are able to photothermally heat aqueous solutions as efficiently as pure Au nanoparticles, even with a 20× smaller concentration of plasmonically actively material. Furthermore, the hybrid structures retain the properties of both materials, creating a multifunctional structure with magnetic and plasmonic properties. While such structures are interesting for biomedical applications, additional uses can be envisioned and are currently being pursued.

ACKNOWLEDGEMENTS

The financial support of this work was provided by Department of Energy DOE- Laboratory Directed Research & Development (LDRD) Strategic Initiative Program. We thank Dr. Robert Lascola, Mr. Henry Sessions, and Mr. Charles Shick for providing their time and expertise to assist us with our experiments.

REFERENCES

[1] G.M. Whitesides, Small, 1, 172-179, 2005.
[2] E. Ozbay, Science, 311, 189-193, 2006.
[3] M.E. Stewart, C.R. Anderton, L.B. Thompson, J. Maria, S.K. Gray, J.A. Rogers, and R.G. Nuzzo, Chem. Rev., 108, 494-521, 2008.
[4] C.J. Murphy, A.M. Gole, S.E. Hunyadi, J.W. Stone, P.N. Sisco, A. Alkilany, B.E. Kinard, and P. Hankins, Chem. Comm., 544-557, 2008.
[5] S.E. Hunyadi and C.J. Murphy, J. Mater. Chem., 16, 3929-3935, 2006.
[6] W.H. Hung, M. Aykol, D. Valley, W. Hou, and S.B. Cronin, Nano Lett., 10, 1314-1318, 2010.
[7] Y. He, P. Basnet, S.E.H. Murph, and Y. Zhao, ACS Appl. Mater. Interfaces, 5, 11818-11827, 2013.
[8] T.A. Larson, J. Bankson, J. Aaron, and K. Sokolov, Nanotechnology, 18, 325101, 2007.
[9] S.E.H. Murph, S. Jacobs, J. Liu, T.C.-C. Hu, M. Siegfired, S.M. Serkiz, and J. Hudson, J. Nanopart. Res., 14, 1-13, 2012.
[10] Y.-L. Luo, Y.-S. Shiao, and Y.-F. Huang, ACS Nano, 5, 7796-7804, 2011.
[11] N.C. Bigall, W.J. Parak, and D. Dorfs, Nano Today, 7, 282-296, 2012.
[12] J. Gao, H. Gu, and B. Xu, Acc. Chem. Res., 42, 1097-1107, 2009.
[13] P. Basnet, G.K. Larsen, R.P. Jadeja, Y.-C. Hung, and Y. Zhao, ACS Appl. Mater. Interfaces, 5, 2085-2095, 2013.
[14] Z. Sun, H. Yuan, Z. Liu, B. Han, and X. Zhang, Adv. Mater., 17, 2993-2997, 2005.
[15] H.B. Na, I.C. Song, and T. Hyeon, Adv. Mater., 21, 2133-2148, 2009.
[16] S.-W. Cao, Y.-J. Zhu, M.-Y. Ma, L. Li, and L. Zhang, J. Phys. Chem. C, 112, 1851-1856, 2008.
[17] M. Lévy, C. Wilhelm, J.-M. Siaugue, O. Horner, J.-C. Bacri, and F. Gazeau, J. Phys.: Condens. Matter, 20, 204133, 2008.
[18] K. Kamei, Y. Mukai, H. Kojima, T. Yoshikawa, M. Yoshikawa, G. Kiyohara, T.A. Yamamoto, Y. Yoshioka, N. Okada, and S. Seino, Biomaterials, 30, 1809-1814, 2009.
[19] C.J. Murphy, T.K. Sau, A.M. Gole, C.J. Orendorff, J. Gao, L. Gou, S.E. Hunyadi, and T. Li, J. Phys. Chem. B, 109, 13857-13870, 2005.
[20] K. Jiang, D.A. Smith, and A. Pinchuk, J. Phys. Chem. C, 117, 27073-27080, 2013.
[21] A.O. Govorov, W. Zhang, T. Skeini, H. Richardson, J. Lee, and N.A. Kotov, Nanoscale Res. Lett., 1, 84-90, 2006.
[22] S. Mukherjee, F. Libisch, N. Large, O. Neumann, L.V. Brown, J. Cheng, J.B. Lassiter, E.A. Carter, P. Nordlander, and N.J. Halas, Nano Lett., 13, 240-247, 2012.